Cellulose
DOI 10.1007/s10570-015-0588-0

ORIGINAL PAPER

Vibrational spectral signatures of crystalline cellulose using high resolution broadband sum frequency generation vibrational spectroscopy (HR-BB-SFG-VS)

Libing Zhang · Zhou Lu · Luis Velarde · Li Fu · Yunqiao Pu · Shi-You Ding · Arthur J. Ragauskas · Hong-Fei Wang · Bin Yang

Received: 4 October 2014 / Accepted: 20 February 2015

Abstract Both the C–H and O–H region spectra of crystalline cellulose were studied using the sub-wavenumber high-resolution broadband sum frequency generation vibrational spectroscopy (HR-BB-SFG-VS) for the first time. The resolution of HR-BB-SFG-VS is about 10-times better than conventional scanning SFG-VS and has the capability of measuring the intrinsic spectral lineshape and revealing many more spectral details. With HR-BB-SFG-VS, we found that in cellulose samples from different sources, including Avicel and cellulose crystals isolated from algae *Valonia* (Iα) and tunicates (Iβ), the spectral signatures in the O–H region were unique for the two allomorphs, i.e. Iα and Iβ, while the spectral signatures in the C–H regions varied in all samples examined. Even though the origin of the different spectral signatures of the crystalline cellulose in the O–H and C–H vibrational frequency regions are yet to be correlated to the structure of cellulose, these results lead to new spectroscopic methods and opportunities to classify and to understand the basic crystalline structures, as well as variations in polymorphism of the crystalline cellulose.

Keywords Cellulose Iα · Cellulose Iβ · Avicel · High resolution broadband sum frequency generation vibrational spectroscopy (HR-BB-SFG-VS)

Electronic supplementary material The online version of this article (doi:10.1007/s10570-015-0588-0) contains supplementary material, which is available to authorized users.

L. Zhang · B. Yang (✉)
Bioproduct Sciences and Engineering Laboratory, Department of Biological Systems Engineering, Washington State University, Richland, WA 99354, USA
e-mail: binyang@tricity.wsu.edu

Z. Lu · L. Velarde · L. Fu · H.-F. Wang (✉)
William R. Wiley Environmental Molecular Sciences Laboratory, Pacific Northwest National Laboratory, Richland, WA 99354, USA
e-mail: hongfei.wang@pnnl.gov

Present Address:
Z. Lu
Beijing National Laboratory for Molecular Sciences, Institute of Chemistry, The Chinese Academy of Sciences, Beijing 100190, China

Present Address:
L. Velarde
Department of Chemistry, University at Buffalo, The State University of New York, Buffalo, NY 14260, USA

Y. Pu · A. J. Ragauskas
School of Chemistry and Biochemistry, Georgia Institute of Technology, Atlanta, GA 30332, USA

Present Address:
Y. Pu · A. J. Ragauskas
Department of Chemical and Biomolecular Engineering, The University of Tennessee, Knoxville, TN 37996-2200, USA

Published online: 03 March 2015

Introduction

Understanding the cellulosic biomass recalcitrance at the molecular level is a key step towards overcoming the fundamental barrier to making cellulosic biofuels cost-competitive (Yang et al. 2011). Although plant cell walls are complex and dynamic, recent advances in analytical chemistry and genomics have substantially enhanced our understanding of cellulosic biomass recalcitrance while simultaneously highlighting the remaining knowledge-gaps (Somerville et al. 2004). The basic chemical constituents of biomass are well known in the literature. The predominant polysaccharide of biomass is cellulose, which makes up about 30–50 % of biomass in the form of linear fibrils composed of approximately 30–40 hydrogen-bonded chains of β-(1, 4) glucopyranosides, with a native degree of polymerization (DP) ranging from several hundred to over ten thousand. Cellulose is also the most abundant organic polymer on Earth. In the cellulose structures, a hydrogen bond network exists in intra-chain and inter-chain hydrogen bonding conformations. The intra-chain hydrogen bond connects the ^{6}COH with the ^{2}COH and the ^{3}COH with endocyclic oxygen while the inter-chain hydrogen bond links the ^{3}COH with ^{6}COH (Lee et al. 2013a). Intermolecular hydrogen bonds are parallel to the glycosidic linkage for both types of chains. Due to its hydrogen bonding diversity, cellulose can exhibit various supra-molecular structures, including amorphous, para-crystalline, and crystalline structures.

Among four types of cellulose structures reported in the literatures, namely cellulose I, II, $III_{I,II}$, and $IV_{I,II}$, cellulose I is the only form that exists in nature (Hayashi et al. 1975). Furthermore, native cellulose I has been shown to be composed of two distinct crystalline forms, referred to as the Iα and the Iβ forms (Atalla and David 1984). Cellulose Iα is triclinic parallel crystalline with only one repeating cellobiose in the unit cell; while Iβ has a monoclinic parallel-down crystalline structure (Henri Chanzy 1985). The relative amounts of Iα and Iβ forms vary significantly among cellulose samples from different origins. For example, cellulose Iα is the dominant form in algae and bacterial cellulose while cellulose Iβ dominates in tunicate and higher plants (Atalla and David 1984). Cellulose materials isolated from different organisms and the methods used to isolate them may result in a variety of different forms with different physio-chemical properties such as crystal size, shape, DP, and crystallinity (Habibi et al. 2010). Previously, structures of cellulose Iα and Iβ were characterized with CP/MAS ^{13}C NMR (Atalla and David 1984; Nishiyama et al. 2002, 2003), and molecular dynamics simulations. Other cellulose structures with different crystalline packing forces and orders have not been studied in details (Fernandes et al. 2011; Thomas et al. 2013). These differences in crystalline packing forces and orders affect a variety of chemical and enzymatic reactions with cellulose (Himmel et al. 2007). Thus, investigating crystalline structural characteristics in different cellulose polymorphs is a fundamental step towards understanding the crystalline cellulose structures in relation to the complex behaviors of the enzymatic hydrolysis in bioconversion of biomass.

Many cellulose characterization techniques have been used to image and characterize the biomass materials, including: (a) atomic force microscopy (AFM), which allows researchers not only to investigate structures of different layers but also to characterize the topographic structures of the cell wall surface (Ding and Liu 2012; Lahiji et al. 2010); (b) high resolution solid state CP/MAS ^{13}C NMR, which is used for quantitative analysis of structural features of cellulose, especially of the crystalline allomorph and disordered domains. The line-shape spectral fitting analysis of solid-state NMR spectra allows a detailed comparison and characterization of the cellulose supra-molecular structures, and this approach has been extensively used to investigate the structural characteristics of cellulose (Pu et al. 2013; Samuel et al. 2010). Cellulose Iα and Iβ were first identified by ^{13}C NMR (Atalla and David 1984). However, ^{13}C CP/MAS NMR results are usually interfered by other materials such as lignin, hemicellulose, and pectin that are usually present in the biomass (Larsson et al. 1999).

In addition to solid-state nuclear magnetic resonance (NMR), native cellulose polymorphism, crystallinity, hydrogen bonding, and mechanical strength

S.-Y. Ding
Biosciences Center, National Renewable Energy Laboratory, Golden, CO 80401, USA

Present Address:
S.-Y. Ding
Department of Plant Biology, Michigan State University, East Lansing, MI 48824-1312, USA

were also studied with IR and Raman vibration spectroscopy (Zugenmaier 2007) and X-ray diffraction (XRD) (Dick-Pérez et al. 2011; Isogai et al. 1989; Liang and Marchessault 1959; Lynette et al. 2002; Mann and Marrinan 1958; Marrinan and Mann 1956; Morikawa et al. 1978; Nelson and O'Connor 1964; Newman et al. 1994; Tsuboi 1957). XRD has been widely applied to quantify and identify the cellulose crystalline structure. However, the crystallinity index (CrI) calculated from XRD varied depending on the calculation methods (Park et al. 2010). In IR and Raman studies on cellulose materials, specific spectral signatures of cellulose with different crystallinity have not been well distinguished from existing IR or Raman spectra (Zugenmaier 2007). Moreover, quantified crystallinity results from different characterization techniques are not always unique or consistent with each other when using different vibrational peaks. For example, Schenzel et al. reported a spectral deconvolution method using bands at 1462 and 1481 cm^{-1} (Schenzel et al. 2005), while other researchers applied different peaks to deconvolute the bands, which led to inconsistent results. Due to complex network of cellulose with other polymers as well as different growing environments of cellulose species, cellulose structural information from these techniques is often affected by other amorphous polysaccharide components. Therefore, isolation and purification of cellulose from biomass are usually required before applying these techniques. However, the isolation and purification process can affect cellulose structures, thus making the characterization of native cellulose a difficult undertaking. Therefore, in order to avoid the interfering effects caused by other biopolymers in the biomass and the tedious cellulose isolation process, a non-destructive spectroscopic technique that can selectively probe the cellulose crystallinity is required to characterize the biomass materials.

Recently, SFG-VS was used to study the physiochemical properties of crystalline cellulose, as the crystalline cellulose exhibits enormous nonlinear optical responses (Barnette et al. 2011, 2012; Kafle et al. 2013; Kim et al. 2013; Lee et al. 2013a, c; Park et al. 2013; Lee et al. 2014a). SFG-VS is a second-order nonlinear spectroscopic method sensitive to the structural symmetry of the molecules and molecular assembly, such as the cellulose crystalline units. Therefore, it has shown great potential in studying cellulose microfibril arrangement and orientation at different stages of plant growth as well as from different sources (Kafle et al. 2013). In this study, four different types of cellulose were probed with the recently developed sub-wavenumber high-resolution broadband sum frequency generation vibrational spectroscopy (HR-BB-SFG-VS) in both the C–H and O–H stretching vibration frequency regions. The advantage of the HR-BB-SFG-VS over the scanning SFG-VS used in previous works is the improvement of the spectral resolution by one order of magnitude, which makes resolving and identifying more detailed spectral features possible. In this study, samples with known and well-characterized crystalline structures, such as Avicel, cellulose Iα and cellulose Iβs from different sources, were chosen in order to establish explicit spectral signatures to differentiate the cellulose Iα and cellulose Iβ crystalline cellulose forms. The determination of the structural differences and similarities between two basic polymorphs cellulose Iα and cellulose Iβ, as well as different sources of cellulose Iβs, can help establish a solid foundation for developing a reliable methodology and metrics to identify cellulose structural variance and quantify the extent of changes during cellulose chemical treatments or enzymatic hydrolysis. Results of this study will aid in the investigation of complexity and uncertainty of cellulose I polymorphs by revealing new information about cellulose structures.

In SFG-VS measurement, usually a visible laser beam with a fixed frequency (ω_{vis}) and an infrared (IR) laser beam with tunable frequency or broadband frequencies (ω_{IR}) simultaneously interact with the material to generate a signal at the sum of the two frequencies ($\omega_{SFG} = \omega_{vis} + \omega_{IR}$) that describe the vibrational spectra of the material. By tuning the IR frequency, the SFG vibrational spectra of the interested material can be measured. SFG-VS is distinct from the IR and Raman spectroscopy because SFG has unique symmetry properties as a result of the second order nonlinear process. Such symmetry properties require the molecule or molecular assembly in the materials that generates SFG signal without centrosymmetry, in other words, the material is either a non-centrosymmetric crystalline material or a molecular surface/interface where the molecules are aligned due to asymmetric forces at the surface/interface) (Shen 1984, 1989). For bulk amorphous solids or liquids, SFG-VS is surface/interface selective, i.e. forbidden for the bulk of materials because

the dominant SFG-VS signals can only come from the surface or interfaces. In the past two decades, SFG-VS was extensively used to probe molecular surfaces and interfaces (Eisenthal 1997; Shen 1994; Wang et al. 2005a). However, in recent years, it has also been found to be useful in selective probe or detection of crystalline materials such as energetic and explosive materials as well as crystalline cellulose (Asher and Willard-Schmoe 2013; Kim et al. 2006; Surber et al. 2007).

The SFG signal is proportional to the intensity of the visible and IR laser intensity ($I(\omega_{VIS})$ and $I(\omega_{IR})$) as well as the square of the effective susceptibility ($\chi^{(2)}_{eff}$) of the material. That is (Shen 1989; Wang et al. 2005a; Zhuang et al. 1999),

$$I(\omega_{SFG}) \propto \left|\chi^{(2)}_{eff}\right|^2 I(\omega_{VIS}) I(\omega_{IR}) \tag{1}$$

$\chi^{(2)}_{eff}$, which contains all the structural and molecular nonlinear optical information of the material, is proportional to the number density of the molecules (N) and is a linear function of the SFG susceptibility tensor χ_{ijk} that is a structural and ensemble orientational average $\left(\left\langle \beta_{i'j'k'} \right\rangle\right)$ of the molecular polarizability tensor $\beta_{i'j'k'}$, that has a frequency dependence on the intrinsic vibrational frequency of the molecules in the material (Zhuang et al. 1999; Wang et al. 2005a; Velarde and Wang 2013a).

$$\chi_{ijk} = N_s \sum_{i'j'k'} \left\langle \beta_{i'j'k'} \right\rangle \tag{2}$$

$$\beta_{i'j'k'} = \beta_{NR,i'j'k'} + \sum_q \frac{\beta_{q,i'j'k'}}{\omega_{IR} - \omega_q + i\Gamma_q} \otimes e^{-\frac{\omega^2_{IR}}{2\Delta\omega^2_q}} \tag{3}$$

$$\beta_{q,i'j'k'} = -\frac{1}{2\varepsilon_0 \omega_q} \frac{\partial \alpha_{i'j'}}{\partial Q_q} \frac{\partial \mu_{k'}}{\partial Q_q} \tag{4}$$

here $\beta_{i'j'k'}$ is the molecular polarizability tensor that consists of a non-resonant contribution $\beta_{NR,i'j'k'}$ and is frequency dependent on the vibrational frequency ω_q (with a homogeneous width $2\Gamma_q$ and an inhomogeneous width $2.35\Delta\omega_q$) of the qth vibrational modes of the molecule (Velarde and Wang 2013a). Here, (i, j, k) and (i', j', k') represent the axis of the (x, y, z) or (x′, y′, z′) coordinates system for the laboratory or the molecular frame, respectively. The mode specific amplitude factor $\beta_{q,i'j'k'}$ is proportional to the molecular Raman tensor $\frac{\partial \alpha_{i'j'}}{\partial Q_q}$ and IR transition dipole vector $\frac{\partial \mu_{k'}}{\partial Q_q}$, where Q is the normal mode coordinates of the qth mode. Therefore, the SFG response can only come from the mode that is both Raman and IR active. All these equations not only provide the way to understand the molecular origin of the SFG spectra, but they also provide the framework to compute or calculate the SFG response from the individual molecular property (through calculate $\beta_{q,i'j'k'}$) and molecular unit structure and ensemble average (through calculate $\left\langle \beta_{i'j'k'} \right\rangle$). The values of the $\beta_{i'j'k'}$ and χ_{ijk} tensors are the result of the microscopic and macroscopic structure and symmetry properties, thus they can be used to determine the structure and interactions of the molecular and overall structure of the material.

Since the number of molecules contributing to the SFG-VS signal from the surface or interface is much smaller than that of crystalline materials, usually the SFG-VS signal from crystalline materials is at least one order or a few orders of magnitude stronger than that from the surface. In addition, since the amorphous material generally has no SFG response, SFG-VS is capable of selectively probing crystalline materials embedded in the amorphous materials (Barnette et al. 2011, 2012). This is the clear advantage of SFG-VS as a selective probe of crystalline cellulose over IR or Raman spectroscopy, both of which probe the crystalline and amorphous material indiscriminately. There is also a different polarization dependence between the SFG-VS signal from the surface and the crystalline materials.

As the symmetry of crystalline material and surface is different, the ensemble average of the SFG responses from the crystalline material and the surface has significantly different polarization dependence. Therefore, these properties can be used to distinguish and determine whether the SFG signal is from the crystalline material or surface when the origin of the SFG signal cannot be easily distinguished. In SFG-VS, the polarization angle corresponding to the zero (null) SFG intensity is called the polarization null angle (PNA). In general, the SFG from bulk crystalline material does not have a null angle, while the SFG signal from a surface usually has a clear null angle (Velarde and Wang 2013b). Therefore, PNA measurement can be used to determine whether the SFG

signal is from the crystalline material or from the surface.

Kim et al. used a commercial picosecond scanning SFG-VS system with spectral resolution about 6 cm^{-1}, and successfully demonstrated the reliable ability of SFG to detect the crystalline structure of cellulose (Barnette et al. 2011, 2012; Lee et al. 2013a). Also, density functional theory with dispersion corrections (DFT-D2) was performed to simulate SFG vibration frequencies of laterally aligned cellulose Iα and Iβ crystals (Lee et al. 2013b). These works reported on the C–H stretching vibrational modes even though the O–H stretching vibrational spectra with the resolution of SFG-VS at 6 cm^{-1} (Barnette et al. 2011; Kim et al. 2013; Lee et al. 2013a, b).

Recently, our team developed a high-resolution broadband sum frequency generation vibrational spectrometer (HR-BB-SFG-VS) with sub-wavenumber spectral resolution that can provide an accurate spectral lineshape and more spectral details in SFG-VS studies with resolution of 0.6 cm^{-1} (Velarde and Wang 2013a, b, c; Velarde et al. 2011). This development has provided new opportunities in improved measurement and better understanding of the SFG spectra and the surface/interface structure and interactions. In this study, four different types of cellulose were probed with HR-BB-SFG-VS in both the CH and OH stretching vibration frequency regions. We chose the samples with known and well-characterized crystalline structures, such as Avicel, cellulose Iα and cellulose Iβs from different sources, in order to establish explicit spectral signatures to differentiate the cellulose Iα and the cellulose Iβ crystalline cellulose forms. The determination of the structural differences and similarities of two basic polymorphs (i.e. cellulose Iα and cellulose Iβ) as well as different sources of cellulose Iβs can help establish a solid foundation for developing reliable methodology and metrics to identify cellulose structural variance and quantify the extent of changes during cellulose chemical treatments or enzymatic hydrolysis. We expect the new information in HR-BB-SFG-VS spectra to improve in-depth interpretation of basic cellulose crystal structures. In this study, characteristic peaks were determined using HR-BB-SFG-VS. The detailed spectral information provided clues for investigating Avicel composition of cellulose Iα and cellulose Iβ, and a PNA measurement was also performed to verify that the measured SFG signal indeed originated from the crystal structure.

Materials and methods

Cellulose samples

Cellulose crystals (cellulose crystals *Valonia* and cellulose crystals tunicate) were prepared according to reported methods (Lee et al. 2013b; Nishiyama et al. 2002, 2003). Cellulose crystals *Valonia* (*CCV*) were isolated from alga *Valonia ventricosa* (Glaucocystis (*nostochinearum*)) cell walls (Imai et al. 1999). Ethanol extraction, alkali and acid treatments were carried out in sequence to produce cellulose Iα. ^{13}C NMR analysis results showed that the cellulose Iα fraction was found to be as high as 90 % (Imai et al. 1999). Two cellulose crystals tunicate (CCT) samples from different sources were used in this study. One was produced from tunicate (*Halocynthiaroretzi*) cellulose (Yoshiharu et al. 1997). The sample was initially treated with aqueous KOH and sodium chloride several times and became colorless. Then strong sulfuric acid hydrolysis was carried out at 40 °C for 8 h while being stirred The suspension was further processed to form cellulose microcrystals (Liang and Marchessault 1959). Another source of cellulose Iβ was isolated from red reef tunicate (*Rhopalaea abdominalis*) (Sugiyama et al. 1992). The red reef tunicates (That Fish Place, http://www.thatpetplace.com/pet/prod/235370/product.web) were slit open with a sharp knife and their mantles were thoroughly washed with deionized water. The whole mantles were soaked overnight in a 5 % (w/v) aqueous KOH solution at room temperature. The mantles were then rinsed with deionized water and bleached for 6 h at 70 °C with a bleaching solution, which was replaced every 2 h. The bleaching solution consisted of 300 mL of chlorite solution (containing 6 g $NaClO_2$) mixed with 5 mL of glacial acetic acid. After repeating the KOH bleaching treatment 4 times, the mantles became completely white and were then washed thoroughly. Avicel PH-101 (11365) was purchased from Fluka BioChemika (Ireland).

HR-BB-SFG-VS

The details of the experimental setup for sub-wavenumber HR-BB-SFG-VS and FID-SFG intensity measurements were previously described (Velarde and Wang 2013a; Velarde et al. 2011). Briefly, to make HR-BB-SFG-VS possible, one needs to generate

well synchronized sub- 100 fs IR pulses and ~100 ps 800 nm pulses. The sub 100 fs IR pulses provide broad IR spectral coverage and the ~100 ps 800 nm pulse provides the sub-wavenumber spectral resolution. This is achieved by electronically synchronizing the two sets of Ti: Sapphire oscillators/amplifiers at a 1 kHz repetition rate running at 40 fs and ~100 ps pulses at the fundamental (800 nm), respectively. This system was constructed with lasers from Coherent, Inc. Both lasers produce 800 nm laser pulses, one with >3.5 W power at ~90 ps pulse width and the other with >7.5 W at ~40 fs. The overall timing jitter between the two synchronized laser pulses is estimated to be <250 fs. In the HR-BB-SFG-VS experiment, about half of the fundamental output generated by the ps amplifier (~90 ps, as measured by cross-correlation) was further attenuated by a variable neutral density filter to ~60 μJ/pulse and used as the source of VIS radiation. The incident angle of the VIS beam (800 nm) was $\beta_{VIS} = 45°$ and the IR beam incident angle was $\beta_{IR} = 56°$ with respect to the surface normal. The SFG signal was collimated by an achromatic lens and isolated from the VIS and IR beams with the combination of an optical iris, an 800 nm notch filter, and a 785 nm shortpass filter (Semrock Inc.). The SFG signal was polarization selected and imaged onto the spectrometer slit (typically open to <100 μm) of a 750 mm spectrograph (Andor Shamrock). The SFG signal was dispersed by a 1200 lines/mm grating and recorded by a thermoelectrically cooled (−80 °C) Electron-Multiplied CCD camera (Andor Newton 971P, back-illuminated) containing a 1600 × 400, 16 μm^2, pixel array. In the HR-BB-SFG-VS measurement, usually a 2-min exposure for the ssp polarization combination was used. Here, the ssp polarization combination is defined as with s-, s-, p-polarization corresponding to the polarization of the optical fields of the SFG signal, visible, and IR beams, respectively (Velarde and Wang 2013c). p polarization is defined when the electric field vector is parallel to the plane of incidence within the incident plane formed by the incident beam direction and the surface normal, and s polarization is perpendicular to the incident plane. Background noise spectrum was measured by delaying the ps VIS and fs IR pulses by >1 ns. The spectra were normalized with the SFG profile from the top surface of a thick Z-cut α-quartz crystal. In comparison to the spectral resolution of the conventional BB-SFG-VS (~15 cm^{-1}) and the scanning SFG-VS (~6 cm^{-1}) in the literature, the HR-BB-SFG-VS in this study has a spectral resolution of ~0.6 cm^{-1}. As demonstrated recently, such significant improvement of the spectral resolution not only enables the ability to resolve closely overlapping peaks (Velarde et al. 2011), but it also provides accurate and intrinsic spectral lineshapes that are crucial for the quantitative spectral and coherent vibrational dynamics analysis of the molecular vibration both at surfaces/interfaces and in non-centrosymmetric crystalline material (Velarde and Wang 2013a, c; Velarde et al. 2011). This study is the first application of HR-BB-SFG-VS in the study of crystalline materials, such as crystalline cellulose.

Polarization null angle measurement with picosecond scanning SFG-VS

A polarization dependent scanning SFG-VS measurement was also performed with the picosecond scanning SFG-VS system (EKSPLA, Inc.), pumped by an Nd:YAG laser with a 50 Hz repetition rate and ~30 ps pulse width. This system is similar to the system used in previous cellulose studies (Barnette et al. 2011). The resolution of the system was ~6 cm^{-1}. The picosecond SFG was carried out in the scanning mode. IR (energy 180 μJ) and visible (energy 100 μJ) beams overlapped on the surface of the sample with an IR incident angle of 56° and a visible incident angle of 45°. The SFG signal was detected with a monochromator and a photomultiplier controlled by a PC computer.

In the PNA measurement, the SFG signal polarization was kept at −45° with respect to the p-polarization direction, and IR polarization was fixed at 0° (p-polarized). The IR wavelength was kept at the strongest band peak at ~2956 cm^{-1}. The polarization angle of the visible beam was changed with a rotating half-wave plate from −45° to 360° (Velarde and Wang 2013c). As shown below, there was no apparent polarization dependence for the SFG-VS signal from all cellulose samples, indicating that the SFG-VS was indeed generated by the bulk of the crystalline material rather than the surface of these materials.

Atomic force microscopy (AFM)

AFM was performed in air using the method reported previously (Ding et al. 2006). A multimode scanning

probe microscope (SPM) with a NanoScope V controller (Veeco, Santa Barbara, CA, USA) was utilized for all AFM measurements. To ensure stability, the AFM was situated in a specially designed laboratory with acoustic and vibration isolation. A customized Nikon optical microscope with deep focus (maximum 800 × magnification) was used to aid the positioning of the AFM tip to the desired face and location on the cell wall. A standard 15-μm scanner was used with the ScanAsyst™ imaging mode and probes. SCANASYST-AIR was used for imaging in air, and SCANASYST-FLUID+ was used for imaging in fluid (Bruker, Camarillo, CA, USA). The software Nanoscope Analysis v1.4 was used for AFM operation and image processing. The AFM imaging recorded many parameters, while all images presented in this study are height images that were flattened at the 3rd order and filtered with a low pass filter.

Results and discussion

Polarization null angle (PNA) testing

Typical PNA method in SFG-VS determines the relative phase and amplitude ratio between the ssp and ppp polarization combination of SFG response (Velarde and Wang 2013c). Figure 1 shows the SFG PNA measurements of cellulose Iα, cellulose Iβ, and Avicel. The SFG intensity at 2956 cm^{-1} consistently showed a flat response under different visible beam polarization angles in Avicel, cellulose Iα, and cellulose Iβ. The lack of a null signal in the whole range of polarization angles for all the samples indicates that the SFG signals of Avicel, cellulose Iα, and cellulose Iβ materials are polarization-independent, i.e. not sensitive to the polarizations of the incident laser beams. Such results suggested that the SFG signals detected from these samples indeed originated from the bulk crystalline structure rather than from the amorphous domain surface (Velarde and Wang 2013c). Another indication that these signals were from crystalline bulk is that the SFG signal was more than two orders of magnitude stronger than the surface SFG signal with full monolayer coverage, such as the air/DMSO interface. Since the SFG signal is not sensitive to polarization angles and the bulk crystalline origin, the polarization dependent measurement that is usually conducted on molecular surfaces is not necessary. Therefore, the SFG measurements in this study were carried out by only applying the commonly used ssp polarization.

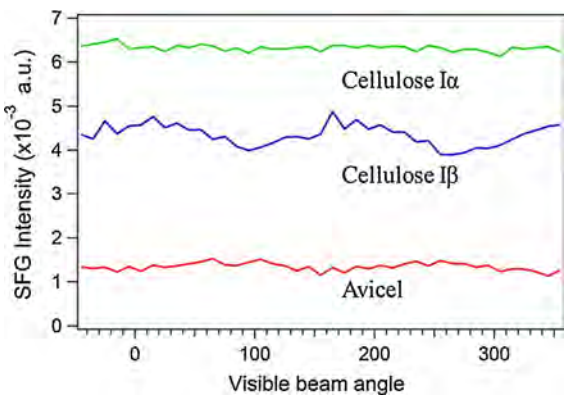

Fig. 1 PNA for different visible polarization angles of cellulose Iα from alga *Valonia ventricosa* (Glaucocystis (*nostochinearum*)), cellulose Iβ from *Halocynthiaroretzi* tunicate, and Avicel using scanning SFG system at 2956 cm^{-1}

HR-BB-SFG-VS spectra of cellulose Iα, Iβ and Avicel samples

SFG-VS was applied to study cellulose microfibril assembly (Lee et al. 2013b) and can serve as an important tool in cellulose structure characterization. Uniaxial-aligned cellulose Iα and Iβ were previously studied by resolution of 6 cm^{-1} (Lee et al. 2013b). However, the spectral differences between the two natural crystals Iα and Iβ from different sources have not been well established. In order to do so, HR-BB-SFG-VS with 0.6 cm^{-1} spectral resolution was applied in the study to probe Avicel, cellulose Iβ from *Halocynthiaroretzi* tunicate, cellulose Iβ from red tunicate, and cellulose Iα from alga *V. ventricosa* (Glaucocystis (*nostochinearum*) in the frequency range of 2700 cm^{-1}–3450 cm^{-1}. The HR-BB-SFG-VS spectra in both the C–H and O–H stretching vibration frequency ranges demonstrated a comprehensive SFG profile of cellulose from different sources (Fig. 2a). Since SFG spectral features require a vibrational mode to be both IR and Raman active, not all peaks seen in IR and Raman spectra were necessarily observed in SFG-VS (Lee et al. 2013b). In the SFG-VS spectra, the spectral differences in C–H and O–H stretch regions are evident among different cellulose samples, including peak positions, intensities, and spectral shapes. These

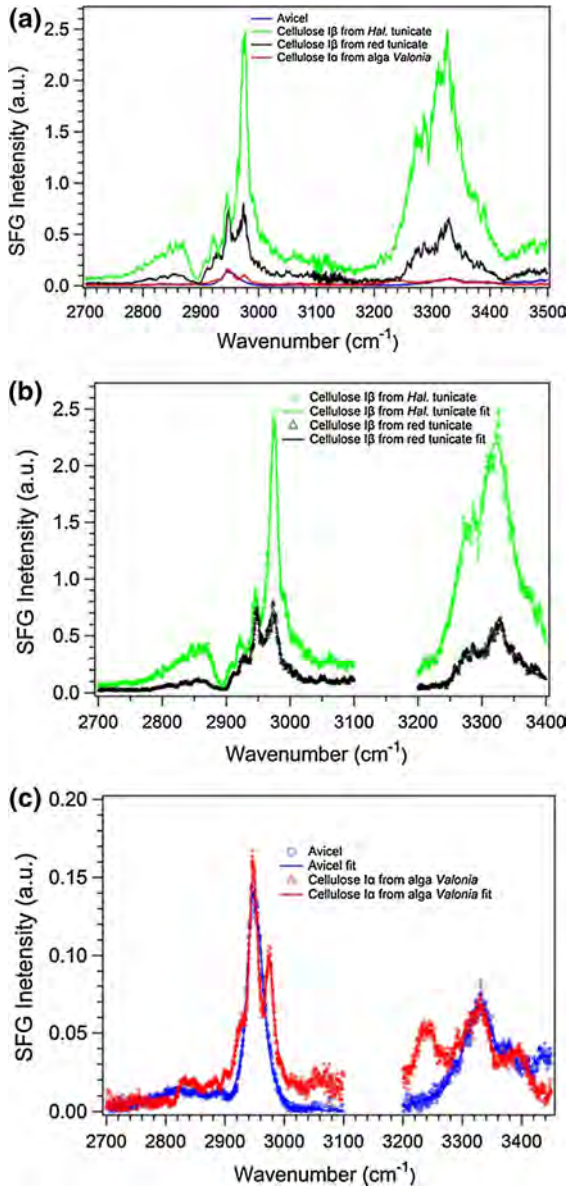

Fig. 2 **a** Experimental HR-BB-SFG-VS spectra of Avicel, cellulose Iβ from *Halocynthiaroretzi* tunicate, cellulose Iβ from red tunicate, and cellulose Iα from alga *Valonia ventricosa* (Glaucocystis (*nostochinearum*)) at wavelengths of 2700–3450 cm^{-1}. All spectra intensities were normalized and presented on the same intensity scale. **b** Spectra for two cellulose Iβs after peak fitting via Lorentz profile convoluted with a Gaussian intensity distribution method; **c** spectra for cellulose Iα (*left axis*) and Avicel (*right axis*)

significant spectral differences enable the identification of different types of cellulose, as discussed below. Spectral fittings were performed to reveal the accurate real peak positions, amplitude, and bandwidth (Fitting results are listed in Table S1 in supplemental materials). Theoretically, SFG peaks can be fitted into Lorentz models convoluted with Gaussian intensity distribution (Eq. 3) (Velarde and Wang 2013a; Wang et al. 2005a), which determines amplitude and other peak shape information (Wang et al. 2005b). However, Lorentzian lineshape is used in SFG-VS fitting in most cases. Figure 2b and c display the fitting results of both CH and OH stretch regions of Iβ and Iα by applying commonly used Lorentzian lineshape function, respectively.

Previous SFG-VS studies characterizing the polymorphism of crystalline cellulose mostly focused on the C–H stretching vibration frequency region. In the literature, it was shown that the spectral features in the surface SFG-VS did not simply follow the IR and Raman spectral assignments, while the assignments in the IR and Raman studies in these spectral regions were not always correct, and the SFG-VS spectral assignment can be achieved with a set of polarization selection rules (Lu et al. 2004, 2005; Wang et al. 2005a). However, the SFG-VS peak assignments are challenging for crystalline materials because the polarization selection rules (Wang et al. 2005a) developed for the surface SFG-VS cannot be directly applied to the SFG-VS spectra from crystalline materials, as the SFG signal from randomly oriented crystalline domains lacks polarization dependence. In previous studies based on IR or Raman literatures, a cellulose peak at 2945 cm^{-1} was assigned to the CH_2 asymmetric vibration of exocyclic $^6CH_2OH$, and peaks in the range of 3100–3500 cm^{-1} were assigned to the OH vibrational region (Barnette et al. 2011). Some of these assignments may not be entirely correct, and the proper assignment of the cellulose SFG-VS spectral peaks is an issue that warrants further study.

Figure 2 indicates that more peaks, such as the 2913, 2930, 3007 and 3377 cm^{-1} peaks, were detected by HR-BB-SFG-VS spectra compared to what was previously reported (Lee et al. 2013c). This phenomenon is the result of the higher spectral resolution in the HR-BB-SFG-VS measurement, which allows detection of intrinsic spectral lineshape without instrument broadening. As a result, more detailed vibrational stretch peaks can be identified, especially with the help of curve fitting results of the HR-BB-SFG-VS spectra [see supplementary Table 1(a, b, c, d)]. These data warrant future studies in understanding the detailed crystalline structure and interaction.

Morphology of cellulose Iα and cellulose Iβs from AFM image

AFM can obtain high-resolution images to reveal lateral packing of the chains. AFM images of four cellulose samples were taken to provide detailed morphological structure and arrangement of the microfibrils measured with HR-BB-SFG-VS. Figure 3 compares AFM images of (a) Avicel, (b) cellulose Iα, and (c, d) two cellulose Iβs, respectively, taken under the same nanoscale resolution. AFM images show similar morphological structures of cellulose microfibrils from *Valonia* and tunicates (Fig. 3b–d), which are relatively larger crystals (20–40 nm in dimensions) that differ from Avicel with small microfibrils (3–5 nm). Cellulose sample from red reef tunicate (C) appears to contain some amorphous structures. Also, Fig. 3 presents different microfibril lateral packing information of Avicel, cellulose Iα and cellulose Iβs, which showed randomly oriented cellulose crystals, different densities of microfibrils, and microfibril packing forms. The two cellulose Iβ samples showed similar microfibril stacking but different microfibril density. All these phenomena reveal the complexity of cellulose microfibril arrangements including fibrils overlapping, twisting and packing forms among four samples. The packing of microfibrils provides information about the nature of the enzyme complexes responsible for oriented cellulose synthesis during plant growth (Thomas et al. 2013; Ding et al. 2013), cellulose specification, and cellulose extraction methods.

The differences in the microfibril packing of the four celluloses are also reflected in the HR-BB-SFG-VS spectra. As shown in Fig. 2a, the SFG intensity of the cellulose Iβ from *Halocynthiaroretzi* tunicate sample has the highest SFG intensity, followed by the cellulose Iβ from red tunicate, the cellulose Iα from alga *V. ventricosa*, and Avicel. Since the SFG signal should be roughly proportional to the density of

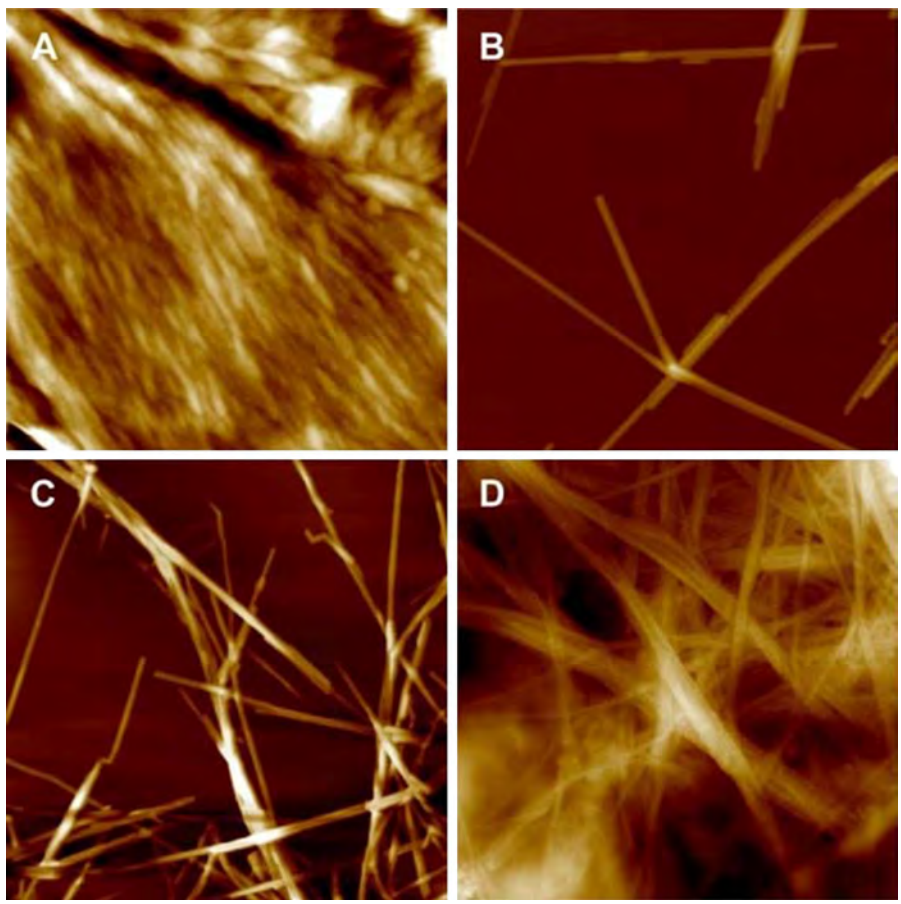

Fig. 3 Comparison of AFM images of **a** Avicel, **b** cellulose Iα from alga *Valonia ventricosa* (Glaucocystis (*nostochinearum*), **c** cellulose Iβ from red tunicate and **d** cellulose Iβ from *Halocynthiaroretzi* tunicate. The scale of all images is 2 × 2 μm

the same microfibrils in the unit volume, it is easy to understand why the cellulose Iβ from *Halocynthiaroretzi* tunicate has the highest SFG intensity and why the cellulose Iβ from red tunicate and the cellulose Iα from alga *V. ventricosa* have smaller SFG intensities, as their microfibril densities in the AFM images in Fig. 3 followed the same decreasing order, e.g. from Fig. 3d, c to b. It is interesting to see that, even though the Avicel sample appears to have a high density from its AFM image (Fig. 3a), its SFG intensity is the smallest and comparable to the cellulose Iα from alga *V. ventricosa*. This fact can only suggest that certain amount of the materials in the Avicel did not contribute to the SFG intensity. In other words, a certain part of the material in the Avicel sample is most likely not in the crystalline cellulose form or it is in an amorphous form that is SFG insensitive. These results suggest that a SFG intensity and cellulose material density correlation might be used to classify the SFG-sensitive crystalline and SFG-insensitive amorphous cellulose materials, and it might also be used to quantify the amount of SFG-sensitive crystalline material in the cellulose material.

Unique O–H signatures for cellulose Iα and cellulose Iβ

The unique spectral signatures for the different forms of crystalline cellulose materials are shown in Fig. 4. These results show that the O–H spectra of two Iβ samples are almost identical in their spectral lineshape even though they have significantly different spectral

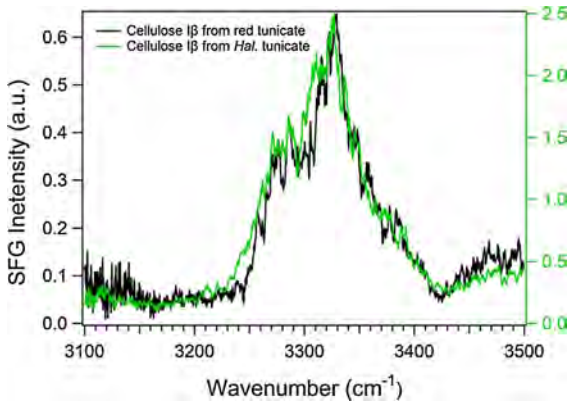

Fig. 4 HR-BB-SFG-VS spectra of cellulose Iβs from *Halocynthiaroretzi* tunicate and red reef tunicate between wavenumber of 3100–3500 cm^{-1}

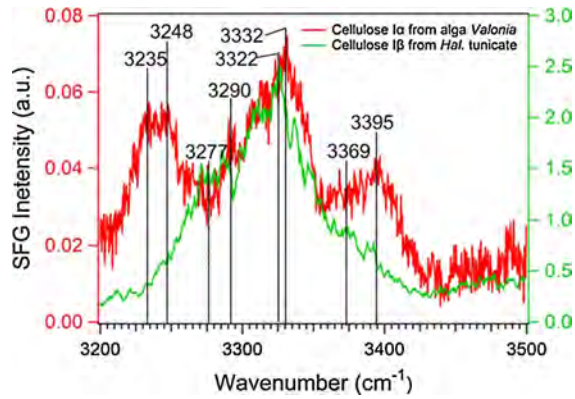

Fig. 5 HR-BB-SFG-VS spectra of cellulose Iβ from *Halocynthiaroretzi* tunicate and cellulose Iα from alga *Valonia ventricosa* (Glaucocystis (*nostochinearum*)) between wavenumber of 3200–3450 cm^{-1}

intensities. In Fig. 5, the Iα and Iβ samples clearly show significantly different spectral lineshapes. Figure 6 shows that the C–H spectra of the two Iβ samples have quite different spectral lineshapes even though the frequency positions of most of their C–H peaks are the same. These results clearly indicate that the O–H spectra features represent the unique signatures that can be used to differentiate the Iα and Iβ forms of crystalline cellulose.

Previous literature reported that the characteristic peaks of cellulose Iα in IR spectra was located at 3240 cm^{-1} (Nishiyama et al. 2003) while cellulose Iβ in IR spectra showed the characteristic peak at 3270 cm^{-1} (Nishiyama et al. 2002). In Fig. 4, two cellulose Iβs from different sources present almost identical peak positions and shapes. It indicates that characteristic peaks of the cellulose Iβs locate in wavenumber ranging from 3100 to 3500 cm^{-1}. Based on peak fitting results, the spectra of the two cellulose Iβs have peak positions at 3277, 3321 and 3369 cm^{-1}.

Figure 5 shows different spectral signatures of the cellulose Iα and cellulose Iβ in terms of both the peak positions and lineshapes. For example, peaks of cellulose Iα are at 3232, 3248, 3290 3304, 3332, and 3395 cm^{-1}, while peaks of cellulose Iβ are at 3277, 3321, and 3369 cm^{-1}. It appears that the 3232, 3248 and 3395 cm^{-1} peaks were unique to the cellulose Iα form while the main 3322 cm^{-1} peak of Iβ overlaps mostly with the 3332 cm^{-1} peak of the Iα form, although it is uncertain whether the amount of Iβ or Iα form is present or dominant. Nevertheless, these

spectral signature differences of the O–H vibrational peaks allow clear identification of cellulose Iβ and cellulose Iα, and they also indicate basic structural differences between the cellulose Iβ and the cellulose Iα in terms of the O–H groups' structure and interactions in their unit cells. It was reported that there were different OH bonds stretch in cellulose Iβ and cellulose Iα allomorphs, which determined the different packing of cellulose chains (Lee et al. 2014a; Kovalenko 2010). The differences in high-resolution SFG spectra of the cellulose Iβ and cellulose Iα samples in this study also reveal the different cellulose microfibril stacking and arrangements. The detailed connection and quantitative correlation of these SFG spectral signatures to the specific crystalline structures of the different crystalline forms warrant further study in the future.

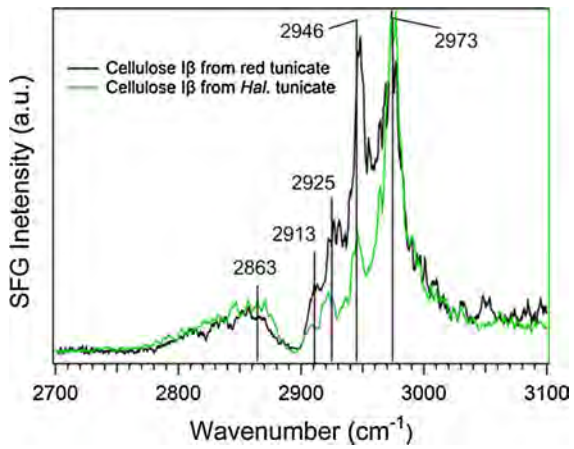

Fig. 6 Difference of cellulose Iβs from red reef tunicate and *Halocynthiaroretzi* tunicate by HR-BB-SFG-VS

CH spectral features for cellulose Iβ samples from different sources

SFG-VS with a resolution of 6 cm^{-1} was previously applied to probe laterally packed and aligned films of cellulose Iα nanowhiskers and cellulose Iβ nanowhiskers, which showed obvious peaks at 2850 and 2944 cm^{-1} and slightly visible peaks at 2886, 2920, and 2988 cm^{-1} (Lee et al. 2013a, 2013b, 2013c). However, the HR-BB-SFG-VS spectra results showed that, even though the two cellulose Iβs had almost identical O–H spectral features, their C–H stretching regions were significantly different (Fig. 6). Dramatic differences of the relative spectral intensities for the two Iβ forms are also identified. In order to compare the relative intensity of different spectral features, the intensities of all peaks in the cellulose Iβs are normalized by the intensity of peak at 2973 $cm^{-1,}$ which is the highest peak in the C–H region. Detailed peak positions, peak amplitudes, and peak widths are shown in the supplemental materials (Table S1). Cellulose Iβs from red reef tunicate and *Halocynthiaroretzi* tunicate show similar peak positions at 2863, 2913, 2925, 2946, 2973, and 2991. Several relative peak intensities of the two cellulose Iβs are prominently similar, but some of them are quite different. For example, the 2946/2973 cm^{-1} amplitude ratio of cellulose Iβ from *Halocynthiaroretzi* tunicate is 0.52, while the ratio of cellulose Iβ from red reef tunicate is 4.08. Such differences indicate that detailed arrangements of the C–H groups in the two cellulose Iβ samples vary. Such differences might be attributed to different microfibril stacking. However, the detailed structural differences need to be further examined in future works.

The two cellulose Iβs were obtained from different species of tunicates and through different cellulose isolation and purification methods, thus they could result in different modification on the cellulose microfibril orientation. Meanwhile, during tunicate growth, microfibrils are also stacked differently. It was demonstrated that the process of cell expansion and/or elongation that occurred during plant development can influence the arrangement of the cellulose elementary fibrils in different plant cell walls (Ding et al. 2013). Therefore, microfibrils are responsible for oriented cellulose synthesis and directional cell expansion during plant growth (Thomas et al. 2013). Therefore, C–H stretching vibrational region might provide critical information in identification of cellulose Iβs from different sources. However, such stacking differences should not alter the O–H interaction in the unit cell of the cellulose Iβ. Otherwise, the O–H spectra of the two forms of Iβ samples should also have been quite different in the peak position or relative intensity.

It is clear that different microfibril stacking structures as well as glucose unit cell structure can result in different vibrational environment for different C–H groups in the cellulose. It is well known that cellulose microfibrils' aggregation significantly influences cellulose crystalline structures. Microfibril is a cellulose

morphological unit that contains a single cellulose elementary fibril (Ding et al. 2013). In the primary plant cell wall, the cellulose elementary fibril is the nascent fibril formed by cellulose synthase rosettes. It was reported that there were six C–H stretching modes in the glucose ring that are detectable with vibrational circular dichroism (VCD) within the wavelength range of 2800–3000 cm^{-1} (Paterlini et al. 1986; Taniguchi and Monde 2007). Therefore, it is not surprising to identify the same, or even higher number of peaks in the HR-BB-SFG-VS spectra of cellulose samples even though the detailed assignment and understanding of their relative intensities can be a challenging task. SFG fields generated form the same molecular group at different positions (either) cancel or enhance each other under the symmetry inversion, which leads to a weaker or stronger peak intensity. Carbons in glucose ring have a different molecular vibration environment that can result in different peak shapes in SFG spectra. Even with high resolution SFG and a higher number of peaks identified, detailed peak assignments and understanding on the six C–H stretching modes are still not quite clear.

Characterization of Avicel probed by HR-BB-SFG-VS

Avicel has been considered to be mainly composed of Iβ and a small portion of Iα (Barnette et al. 2011, 2012). Figure 7 shows the Avicel O–H stretching region SFG spectrum together with the spectra of both the cellulose Iα and the cellulose Iβ. The peak parameters of the three samples after curve fitting are listed in the supplemental materials (Table S1). These results show that Avicel appears to be mostly composed of cellulose Iβ peaks and a small portion of cellulose Iα peaks, although they present some different peak positions and peak shapes compared with the pure cellulose Iβ and cellulose Iα. In an earlier section, results suggested that O–H stretch peaks were characteristic spectral signatures capable of distinguishing cellulose Iα and cellulose Iβ. While Avicel simply had peaks at 3332, 3378, and 3432 cm^{-1}, cellulose Iα had peaks at 3232, 3248, 3290, 3304, 3332, and 3395 cm^{-1}, and cellulose Iβ had peaks at 3277, 3322, and 3369 cm^{-1}. The C–H vibrational region (from 2700 to 3050 cm^{-1}) of cellulose Iα and cellulose Iβs both showed a peak at ~2973 cm^{-1} (Fig. 2a–c). Peak fitting results of C–H region showed

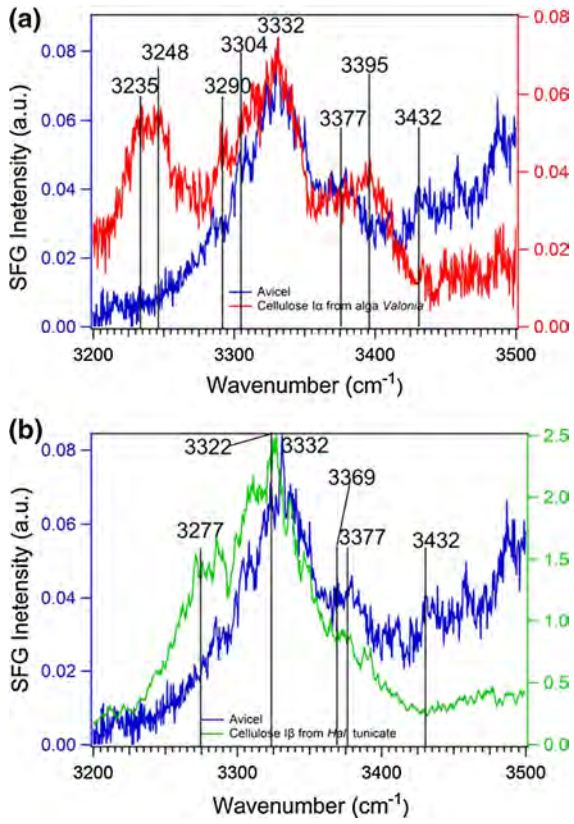

Fig. 7 HR-BB-SFG-VS spectra of Avicel and cellulose Iα from alga *Valonia ventricosa* (Glaucocystis (*nostochinearum*)) (**a**) and cellulose Iβ from *Halocynthiaroretzi* tunicate (**b**), respectively, between wavelengths of 3200–3450 cm^{-1}

that four peaks in the Avicel C–H stretch region at ~2846, ~2895, ~2946 and ~2956 cm^{-1}, which present a more detailed structure than previously reported (Barnette et al. 2011). Since there is no Avicel spectral peak in the 3232 and 3248 cm^{-1} regions, it is unlikely that there is much Iα form present in Avicel. It is therefore reasonable to conclude that Avicel consists of mostly the Iβ form in addition to a certain amount of SFG-insensitive amorphous material. Thus, it appears that, with the high-resolution SFG-VS, the O–H stretch region is a signature that identifies Avicel, cellulose Iα and cellulose Iβ, while C–H vibrational peaks reflect the complex microfibril packing and microfibril composed sheets packing in cellulose structure without manual alignment (Park et al. 2013, 2014; Lee et al. 2014b; Kafle et al. 2014).

Both peak intensity and integrated peak ratios were used to estimate crystalline cellulose and cellulose lateral packing orientation (Park et al. 2010; Barnette

Table 1 Comparison of C–H, O–H peaks areas and their ratios of Avicel, cellulose Iβ (different sources) and cellulose Iα

Samples	C–H peaks area	O–H peak area	R
Cellulose Iβ from *Halocynthiaroretzi* tunicate	147.0	273.0	0.54
Cellulose Iβ from red reef tunicate	366.0	69.3	0.52
Cellulose Iα from alga *Valonia ventricosa* (Glaucocystis (*nostochinearum*))	12.5	11.4	1.10
Avicel	7.0	10.5	0.67

et al. 2012; Lee et al. 2014b; Ma and Allen 2003). However, the intensity ratio might not be accurate enough since some peaks overlapped, thus resulting in miscount issues. For example, ~2913 and ~2925 cm^{-1} of cellulose Iβ are shoulder peaks on top of the main peak at 2946 cm^{-1}. Instead of the intensity ratio of individual peaks, the ratio (R) of the total C–H stretching vibrational peak areas over the total integrated O–H peak areas seem to be useful to evaluate the spectra differences of Avicel, cellulose Iα and cellulose Iβs. Results showed that the R values differ among Avicel, cellulose Iα and cellulose Iβs, while they are similar among the two cellulose Iβs (Table 1). For example, cellulose Iβ from *Halocynthiaroretzi* tunicate has a R value of 0.54 while cellulose Iβ from red reef tunicate has a R value of 0.52, while the R value of cellulose Iα is 1.1. The R value of Avicel (0.67) was closer to that of cellulose Iβ. These results are consistent with previous reports that Avicel is composed of mostly Iβ form (Barnette et al. 2012). It appears that the integrated area ratio might be useful in characterizing cellulose structures.

Conclusion

This is the first report on HR-BB-SFG-VS measurement of cellulose Iα, cellulose Iβ, and Avicel that is used to identify the spectral signatures of different cellulose microfibrils. The findings suggest that the O–H stretching region represents unique spectral signatures that can be used to distinguish cellulose Iα and cellulose Iβ, while the C–H spectral features do not exhibit such explicit correlation to different types of crystalline structures of cellulose. It was also found that the ratios of the total C–H stretching vibrational peak areas over the total integrated O–H peak areas of Avicel, cellulose Iα and cellulose Iβs correlated well to different types of cellulose microfibrils. In addition, many more peaks are identified in the C–H stretching region by the HR-BB-SFG-VS than by the conventional SFG-VS. For example, the peak at ~2945 cm^{-1} was assigned to the CH_2 asymmetric stretching peaks. However, HR-BB-SFG-VS detected another obvious peak at ~2973 cm^{-1} nearby, which is usually not present in the conversional SFG-VS. Such new insights can help us define crystalline cellulose structures in more details and can provide confirmation in measuring spectral lineshape, resolving different spectral peaks. With the detailed spectral information from the HR-BB-SFG-VS measurement, more future work should be expected to focus on peak assignment and illustrating the cellulose structure changes in the cellulose treatment or transformation processes as their detailed SFG-VS spectral features change can be followed. These developments shall make SFG-VS a useful in situ spectroscopic tool, not only in cellulose structure and kinetics studies, but also in other crystalline biopolymer material studies.

Acknowledgments This work was made possible through the support of the DARPA Young Faculty Award Contract # N66001-11-1-414. Authors also acknowledge the support of Bioproducts, Sciences and Engineering Laboratory, Department of Biosystems Engineering at Washington State University. L. Zhang was partially supported by the grant from the Chinese Scholarship Council (CSC). S.Y. Ding was supported by the BioEnergy Science Center, a DOE Bioenergy Research Center, and the Genomic Science Program (ER65258), both supported by the Office of Biological and Environmental Research in the DOE Office of Science. Part of this work was conducted at the William R. Wiley Environmental Molecular Sciences Laboratory (EMSL), a national scientific user facility located at the Pacific Northwest National Laboratory (PNNL) and sponsored by the Department of Energy's Office of Biological and Environmental Research (BER). We also thank Dr. Seong Kim (Penn State University) for insightful discussions.

References

Asher WE, Willard-Schmoe E (2013) Vibrational sum-frequency spectroscopy for trace chemical detection on

surfaces at stand-off distances. Appl Spectrosc 67(3):253–260. doi:10.1366/12-06792

Atalla RHV, David L (1984) Native cellulose: a composite of two distinct crystalline forms. Science 223(4633):283–285. doi:10.1126/science.223.4633.283

Barnette AL, Bradley LC, Veres BD, Schreiner EP, Park YB, Park J, Park S, Kim SH (2011) Selective detection of crystalline cellulose in plant cell walls with sum-frequency-generation (SFG) vibration spectroscopy. Biomacromolecules 12(7):2434–2439. doi:10.1021/bm200518n

Barnette AL, Lee C, Bradley LC, Schreiner EP, Park YB, Shin H, Cosgrove DJ, Park S, Kim SH (2012) Quantification of crystalline cellulose in lignocellulosic biomass using sum frequency generation (SFG) vibration spectroscopy and comparison with other analytical methods. Carbohydr Polym 89(3):802–809. doi:10.1016/j.carbpol.2012.04.014

Dick-Pérez M, Zhang Y, Hayes J, Salazar A, Zabotina OA, Hong M (2011) Structure and interactions of plant cell-wall polysaccharides by two- and three-dimensional magic-angle-spinning solid-state NMR. Biochemistry 50(6):989–1000. doi:10.1021/bi101795q

Ding S-Y, Liu Y-S (2012) Imaging cellulose using atomic force microscopy. In: Himmel ME (ed) Biomass conversion, vol. 908. Methods in Molecular Biology. Humana Press, pp 23–30. doi:10.1007/978-1-61779-956-3_3

Ding S-Y, Xu Q, Ali MK, Baker JO, Bayer EA, Barak Y, Lamed R, Sugiyama J, Rumbles G, Himmel ME (2006) Versatile derivatives of carbohydrate-binding modules for imaging of complex carbohydrates approaching the molecular level of resolution. Biotechniques 41(4):435

Ding S-Y, Zhao S, Zeng Y (2013) Size, shape, and arrangement of native cellulose fibrils in maize cell walls. Cellulose 21(2):863–871. doi:10.1007/s10570-013-0147-5

Eisenthal KB (1997) SFG studies of structural phase transitions at air/water interfaces and shg from the surfaces of microscopic centrosymmetric structures in bulk solution. Abstracts of Papers of the American Chemical Society 213:69-COLL

Fernandes AN, Thomas LH, Altaner CM, Callow P, Forsyth VT, Apperley DC, Kennedy CJ, Jarvis MC (2011) Nanostructure of cellulose microfibrils in spruce wood. Proc Natl Acad Sci 108(47):E1195–E1203. doi:10.1073/pnas.1108942108

Habibi Y, Lucia LA, Rojas OJ (2010) Cellulose nanocrystals: chemistry, self-assembly, and applications. Chem Rev 110(6):3479–3500

Hayashi J, Sufoka A, Ohkita J, Watanabe S (1975) The confirmation of existences of cellulose IIII, IIIII, IVI, and IVII by the X-ray method. J Polym Sci Polym Lett Ed 13(1):23–27. doi:10.1002/pol.1975.130130104

Henri Chanzy BH (1985) Undirectional degradation of valonia cellulose microcrystals subjected to cellulase action. FEBS Lett 184:285–288. doi:10.1016/0014-5793(85)80623-2

Himmel ME, Ding SY, Johnson DK, Adney WS, Nimlos MR, Brady JW, Foust TD (2007) Biomass recalcitrance: engineering plants and enzymes for biofuels production. Science 315(5813):804–807. doi:10.1126/science.1137016

Imai T, Sugiyama J, Itoh T, Horii F (1999) Almost pure I(alpha) cellulose in the cell wall of Glaucocystis. J Struct Biol 127(3):248–257

Isogai A, Usuda M, Kato T, Uryu T, Atalla RH (1989) Solid-state CP/MAS carbon-13 NMR study of cellulose polymorphs. Macromolecules 22(7):3168–3172. doi:10.1021/ma00197a045

Kafle K, Xi X, Lee CM, Tittmann BR, Cosgrove DJ, Park YB, Kim SH (2013) Cellulose microfibril orientation in onion (*Allium cepa* L.) epidermis studied by atomic force microscopy (AFM) and vibrational sum frequency generation (SFG) spectroscopy. Cellulose 21(2):1075–1086. doi:10.1007/s10570-013-0121-2

Kafle K, Shi R, Lee CM, Mittal A, Park YB, Sun Y-H, Park S, Chiang V, Kim SH (2014) Vibrational sum-frequency-generation (SFG) spectroscopy study of the structural assembly of cellulose microfibrils in reaction woods. Cellulose 21(4):2219–2231. doi:10.1007/s10570-014-0322-3

Kim H, Lagutchev A, Dlott DD (2006) Surface and interface spectroscopy of high explosives and binders: HMX and Estane. Propellants Explos Pyrotech 31(2):116–123. doi:10.1002/prep.200600017

Kim S, Lee C, Kafle K (2013) Characterization of crystalline cellulose in biomass: basic principles, applications, and limitations of XRD, NMR, IR, Raman, and SFG. Korean J Chem Eng 30(12):2127–2141. doi:10.1007/s11814-013-0162-0

Kovalenko (2010) Crystalline cellulose structure and hydrogen bonds. Russ Chem Rev 79(3):231–241. doi:10.1070/RC2010v079n03ABEH004065

Lahiji RR, Xu X, Reifenberger R, Raman A, Rudie A, Moon RJ (2010) Atomic force microscopy characterization of cellulose nanocrystals. Langmuir 26(6):4480–4488. doi:10.1021/la903111j

Larsson PTHE, Wickholm K, Pettersson E, Iversen T (1999) CP/MAS 13C-NMR spectroscopy applied to structure and interaction studies on cellulose I. Solid State Nucl Magn Reson 15:31–40

Lee CM, Mittal A, Barnette AL, Kafle K, Park YB, Shin H, Johnson DK, Park S, Kim SH (2013a) Cellulose polymorphism study with sum-frequency-generation (SFG) vibration spectroscopy: identification of exocyclic CH_2OH conformation and chain orientation. Cellulose 20(3):991–1000. doi:10.1007/s10570-013-9917-3

Lee CM, Mohamed NM, Watts HD, Kubicki JD, Kim SH (2013b) Sum-frequency-generation vibration spectroscopy and density functional theory calculations with dispersion corrections (DFT-D2) for cellulose Ialpha and Ibeta. J Phys Chem B 117(22):6681–6692. doi:10.1021/jp402998s

Lee CM, Mohamed NMA, Watts HD, Kubicki JD, Kim SH (2013c) Sum-frequency-generation vibration spectroscopy and density functional theory calculations with dispersion corrections (DFT-D2) for cellulose Ialpha and Ibeta. J Phys Chem B 117(22):6681–6692. doi:10.1021/jp402998s

Lee CM, Kafle K, Park YB, Kim SH (2014a) Probing crystal structure and mesoscale assembly of cellulose microfibrils in plant cell walls, tunicate tests, and bacterial films using vibrational sum frequency generation (SFG) spectroscopy. Phys Chem Chem Phys 16(22):10844–10853. doi:10.1039/c4cp00515e

Lee CM, Kafle K, Park YB, Kim SH (2014b) Probing crystal structure and mesoscale assembly of cellulose microfibrils in plant cell walls, tunicate tests, and bacterial films using vibrational sum frequency generation (SFG) spectroscopy.

Phys Chem Chem Phys 16(22):10844–10853. doi:10.1039/c4cp00515e

Liang CY, Marchessault RH (1959) Infrared spectra of crystalline polysaccharides. II. Native celluloses in the region from 640 to 1700 cm^{-1}. J Polym Sci 39(135):269–278. doi:10.1002/pol.1959.1203913521

Lu R, Gan W, Wu BH, Chen H, Wang HF (2004) Vibrational polarization spectroscopy of CH stretching modes of the methylene group at the vapor/liquid interfaces with sum frequency generation. J Phys Chem B 108(22):7297–7306. doi:10.1021/jp036674o

Lu R, Gan W, Wu BH, Zhang Z, Guo Y, Wang HF (2005) C–H stretching vibrations of methyl, methylene and methine groups at the vapor/alcohol (n = 1-8) interfaces. J Phys Chem B 109(29):14118–14129. doi:10.1021/jp051565q

Lynette M, Daviesa PJH, Newman Roger H (2002) Molecular ordering of cellulose after extraction of polysaccharides from primary cell walls of *Arabidopsis thaliana*: a solid-state CP/MAS 13C NMR study. Carbohydr Res 337(7):587–593. doi:10.1016/S0008-6215(02)00038-1

Ma G, Allen HC (2003) Surface studies of aqueous methanol solutions by vibrational broad bandwidth sum frequency generation spectroscopy. J Phys Chem B 107(26):6343–6349. doi:10.1021/jp027364t

Mann J, Marrinan HJ (1958) Crystalline modifications of cellulose. Part II. A study with plane-polarized infrared radiation. J Polym Sci 32(125):357–370. doi:10.1002/pol.1958.1203212507

Marrinan HJ, Mann J (1956) Infrared spectra of the crystalline modifications of cellulose. J Polym Sci 21(98):301–311. doi:10.1002/pol.1956.120219812

Morikawa H, Hayashi R, Senda M (1978) Infrared analysis of pea stem cell walls and oriented structure of matrix polysaccharides in them. Plant Cell Physiol 19(7):1151–1159

Nelson ML, O'Connor RT (1964) Relation of certain infrared bands to cellulose crystallinity and crystal latticed type. Part I. Spectra of lattice types I, II, III and of amorphous cellulose. J Appl Polym Sci 8(3):1311–1324. doi:10.1002/app.1964.070080322

Newman RH, Ha M-A, Melton LD (1994) Solid-state 13C NMR investigation of molecular ordering in the cellulose of apple cell walls. J Agric Food Chem 42(7):1402–1406. doi:10.1021/jf00043a002

Nishiyama Y, Langan P, Chanzy H (2002) Crystal structure and hydrogen-bonding system in cellulose Iβ from synchrotron X-ray and neutron fiber diffraction. J Am Chem Soc 124(31):9074–9082. doi:10.1021/ja0257319

Nishiyama Y, Sugiyama J, Chanzy H, Langan P (2003) Crystal structure and hydrogen bonding system in cellulose Iα from synchrotron X-ray and neutron fiber diffraction. J Am Chem Soc 125(47):14300–14306. doi:10.1021/ja037055w

Park S, Baker JO, Himmel ME, Parilla PA, Johnson DK (2010) Cellulose crystallinity index: measurement techniques and their impact on interpreting cellulase performance. Biotechnol Biofuels 3:10. doi:10.1186/1754-6834-3-10

Park YB, Lee CM, Koo BW, Park S, Cosgrove DJ, Kim SH (2013) Monitoring meso-scale ordering of cellulose in intact plant cell walls using sum frequency generation spectroscopy. Plant Physiol 163(2):907–913. doi:10.1104/pp.113.225235

Park YB, Lee CM, Kafle K, Park S, Cosgrove DJ, Kim SH (2014) Effects of plant cell wall matrix polysaccharides on bacterial cellulose structure studied with vibrational sum frequency generation spectroscopy and X-ray diffraction. Biomacromolecules 15(7):2718–2724. doi:10.1021/bm500567v

Paterlini MG, Freedman TB, Nafie LA (1986) Ring current enhanced vibrational circular dichroism in the carbon-hydrogen bond stretching motions of sugars. J Am Chem Soc 108(7):1389–1397. doi:10.1021/ja00267a005

Pu Y, Hallac B, Ragauskas AJ (2013) Plant biomass characterization: application of solution- and solid-state NMR spectroscopy. In: Wyman CE (ed) Aqueous pretreatment of plant biomass for biological and chemical conversion to fuels and chemicals. Wiley, New York, pp 369–390. doi:10.1002/9780470975831.ch18

Samuel R, Pu Y, Foston M, Ragauskas AJ (2010) Solid-state NMR characterization of switchgrass cellulose after dilute acid pretreatment. Biofuels 1(1):85–90

Schenzel K, Fischer S, Brendler E (2005) New method for determining the degree of cellulose i crystallinity by means of FT Raman spectroscopy. Cellulose 12(3):223–231. doi:10.1007/s10570-004-3885-6

Shen YR (1984) The principles of nonlinear optics. Wiley-Interscience, New York

Shen YR (1989) Surface-properties probed by 2nd harmonic and sum frequency generation. Nature 337(6207):519–525. doi:10.1038/337519a0

Shen YR (1994) Surface spectroscopy by nonlinear optics. Frontiers in laser spectroscopy, vol 120

Somerville C, Bauer S, Brininstool G, Facette M, Hamann T, Milne J, Osborne E, Paredez A, Persson S, Raab T, Vorwerk S, Youngs H (2004) Toward a systems approach to understanding plant cell walls. Science 306(5705):2206–2211. doi:10.1126/science.1102765

Sugiyama J, Chanzy H, Maret G (1992) Orientation of cellulose microcrystals by strong magnetic fields. Macromolecules 25(16):4232–4234. doi:10.1021/ma00042a032

Surber E, Lozano A, Lagutchev A, Kim H, Dlott DD (2007) Surface nonlinear vibrational spectroscopy of energetic materials: HMX. J Phys Chem C 111(5):2235–2241. doi:10.1021/jp066801r

Taniguchi T, Monde K (2007) Vibrational circular dichroism (VCD) studies on disaccharides in the CH region: toward discrimination of the glycosidic linkage position. Org Biomol Chem 5(7):1104–1110. doi:10.1039/B618841A

Thomas LH, Forsyth VT, Sturcova A, Kennedy CJ, May RP, Altaner CM, Apperley DC, Wess TJ, Jarvis MC (2013) Structure of cellulose microfibrils in primary cell walls from collenchyma. Plant Physiol 161(1):465–476. doi:10.1104/pp.112.206359

Tsuboi M (1957) Infrared spectrum and crystal structure of cellulose. J Polym Sci 25(109):159–171. doi:10.1002/pol.1957.1202510904

Velarde L, Wang H-F (2013a) Unified treatment and measurement of the spectral resolution and temporal effects in frequency-resolved sum-frequency generation vibrational

spectroscopy (SFG-VS). Phys Chem Chem Phys. doi:10.1039/C3CP52577E

Velarde L, Wang HF (2013b) Capturing inhomogeneous broadening of the—CN stretch vibration in a Langmuir monolayer with high-resolution spectra and ultrafast vibrational dynamics in sum-frequency generation vibrational spectroscopy (SFG-VS). J Chem Phys 139(8):084204. doi:10.1063/1.4818996

Velarde L, Wang HF (2013c) Unique determination of the—CN group tilt angle in Langmuir monolayers using sum-frequency polarization null angle and phase. Chem Phys Lett 585:42–48. doi:10.1016/j.cplett.2013.07.052

Velarde L, Zhang XY, Lu Z, Joly AG, Wang ZM, Wang HF (2011) Communication: spectroscopic phase and lineshapes in high-resolution broadband sum frequency vibrational spectroscopy: resolving interfacial inhomogeneities of "identical" molecular groups. J Chem Phys 135(24):241102. doi:10.1063/1.3675629

Wang H-F, Gan W, Lu R, Rao Y, Wu B-H (2005a) Quantitative spectral and orientational analysis in surface sum frequency generation vibrational spectroscopy (SFG-VS). Int Rev Phys Chem 24(2):191–256. doi:10.1080/01442350500225894

Wang H-F, Gan W, Lu R, Rao Y, Wu B-H (2005b) Quantitative spectral and orientational analysis in surface sum frequency generation vibrational spectroscopy (SFG-VS). Int Rev Phys Chem 24(2):191–256. doi:10.1080/01442350500225894

Yang B, Dai Z, Ding S-Y, Wyman CE (2011) Enzymatic hydrolysis of cellulosic biomass. Biofuels 2(4):421–450. doi:10.4155/bfs.11.116

Yoshiharu NSK, Masahisa W, Takeshi O (1997) Cellulose microcrystal film of high uniaxial orientation. Macromolecules 30:6395–6397. doi:10.1021/ma970503y

Zhuang X, Miranda PB, Kim D, Shen YR (1999) Mapping molecular orientation and conformation at interfaces by surface nonlinear optics. Phys Rev B 59(19):12632–12640. doi:10.1103/PhysRevB.59.12632

Zugenmaier P (2007) Crystalline cellulose and derivatives: characterization and structures. In: Timell TE, Wimmer R (eds) Wood science. doi:10.1002/bbpc.19850891120